

Article

Xylene and n-Hexane Adsorption Performance of a Waste Methanol-to-Propylene Catalyst under Acid-Base Treatment

Xiaojing Yong^{1,2}, Hui Su², Nana Zhao², Zhengwei Jin², Min Yao^{1,*}  and Yulong Ma^{1,*}

¹ State Key Laboratory of High-Efficiency Utilization of Coal and Green Chemical Engineering, College of Chemistry and Chemical Engineering, Ningxia University, Yinchuan 750021, China

² Institute of Coal Chemical Industry Technology, Ningxia Coal Industry Co., Ltd., National Energy Group, Yinchuan 750411, China

* Correspondence: ndglym@163.com (M.Y.); yulongma796@sohu.com (Y.M.)

Abstract: Spent methanol-to-propylene (MTP) catalysts have a large specific surface area and high porosity but are usually directly disposed of in landfills, and recycling is rare. In this study, spent MTP catalyst was moderately dealuminized with acids and etched with an alkali solvent to increase its specific surface area. A novel adsorbent was obtained. XRD, SEM, FT-IR, XRF, and MAS-NMR characterization shows that the adsorbent maintains a typical ZSM-5 zeolite structure, and the dealumination effect of $\text{H}_2\text{C}_2\text{O}_4$ is better than that of HCl. HCl mainly removes the framework aluminum of the molecular sieve; $\text{H}_2\text{C}_2\text{O}_4$ not only removes the framework aluminum but also dissolves some of the nonframework aluminum, which increases the BET-specific surface area and pore diameter. The spent catalyst maintains an irregular ellipsoidal shape. After alkali treatment, the surface of the spherical particles becomes rough. With increasing alkali concentration, the damage degree increases. After treatment with 4 mol/L $\text{H}_2\text{C}_2\text{O}_4$ and 0.1 mol/L NaOH, the p-xylene and n-hexane adsorption capacities reach the maximum, with values of 141.04 mg/g and 106.87 mg/g, respectively, 20.7% and 16.2% greater than those before treatment. These findings indicate that modified spent MTP catalyst has the potential for application in the removal of VOCs from the air.

Keywords: spent MTP catalyst; ZSM-5; adsorption; p-xylene; n-hexane



Citation: Yong, X.; Su, H.; Zhao, N.; Jin, Z.; Yao, M.; Ma, Y. Xylene and n-Hexane Adsorption Performance of a Waste Methanol-to-Propylene Catalyst under Acid-Base Treatment. *Catalysts* **2022**, *12*, 1028. <https://doi.org/10.3390/catal12091028>

Academic Editors: Maja Milojević-Rakić and Danica Bajuk-Bogdanović

Received: 6 August 2022

Accepted: 5 September 2022

Published: 10 September 2022

Publisher's Note: MDPI stays neutral with regard to jurisdictional claims in published maps and institutional affiliations.



Copyright: © 2022 by the authors. Licensee MDPI, Basel, Switzerland. This article is an open access article distributed under the terms and conditions of the Creative Commons Attribution (CC BY) license (<https://creativecommons.org/licenses/by/4.0/>).

1. Introduction

Methanol-to-propylene (MTP) catalysts are formed of a ZSM-5 molecular sieve. ZSM-5 molecular sieves have a unique pore structure that provides good ion exchange performance and shape selectivity [1–3]. Because of its good thermal stability, hydrothermal stability, wide distribution of Si/Al, and wide range of acid adjustability, ZSM-5 zeolite is a good solid acid catalyst and catalyst carrier [4,5]. It is widely used in catalysis, such as in the petrochemical and coal chemical industries, as well as in the fields of wastewater treatment and selective adsorption [6–9]. Many published studies have reported that MTP catalysts require small grain HZSM-5 molecular sieves with a high Si to Al ratio and a multistage composite pore structure [6,10–12]. Researchers have focused on the design and development of new MTP catalysts [9,13–15], but have rarely studied the comprehensive utilization of functionalized spent MTP catalysts [16,17]. Spent MTP catalysts have a large specific surface area, high porosity, and good adsorption performance [18–20]. In recent years, the massive emission of volatile organic compounds (VOCs) has caused serious harm to the human body and the environment [11,13,21,22]. The porous multistage composite ZSM-5 molecular sieve with an MFI structure can realize the selective adsorption of VOCs on the molecular scale, due to the interconnection of its microporous structure and mesoporous structure [23–27]. This paper systematically investigated the effect of acid-base treatment on the texture properties of waste MTP catalyst, enhanced the adsorption potential of VOCs on a waste molecular sieve, and provided support for the resource utilization of waste catalysts.

2. Results and Discussion

2.1. XRD Characterization of the Adsorbent Products

The XRD spectra of the adsorbent products are shown in Figure 1a,b. The hydrophobic adsorbent products maintain a typical ZSM-5 molecular sieve structure, and the corresponding characteristic peaks of the ZSM-5 (011), (020), (051), and (033), crystal planes appear at $2\theta = 7.9^\circ$, 8.8° , 23.1° , and 23.8° , respectively, which indicates that the adsorbent channels have long-range order [9–12]. Acid treatment did not change the crystal phase structure of the spent catalyst, but the diffraction peak intensity after sample processing increases with increasing acid concentration. This may be caused by the elimination of impurities over the spent catalyst by acid treatment.

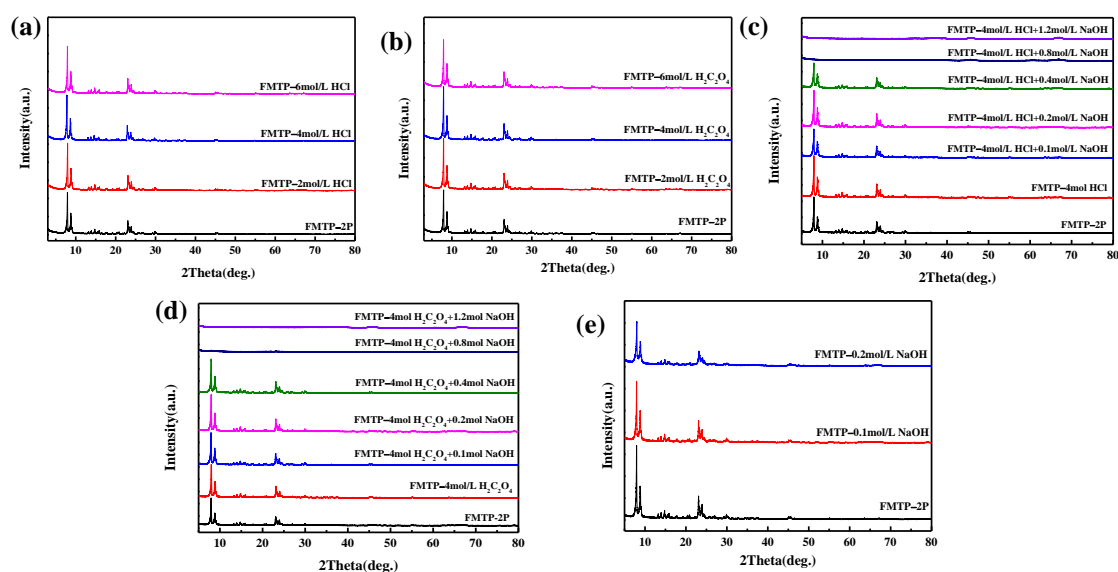


Figure 1. XRD spectra of spent catalyst samples after (a) HCl treatment; (b) $\text{H}_2\text{C}_2\text{O}_4$ treatment; (c) 4 mol/L HCl and alkali combined treatment; (d) 4 mol/L $\text{H}_2\text{C}_2\text{O}_4$ and alkali combined treatment; and (e) alkali treatment.

Figure 1c,d shows that after treatment with different concentrations of alkali, the crystal phase structure of the spent catalyst is not destroyed, no characteristic peaks disappear, and no new diffraction peaks are observed. However, with increasing alkali concentration, the diffraction peak intensity is reduced, which may be due to framework desilication of the spent catalyst and the generation of local structural defects in the molecular sieve lattice, resulting in a decline in the intensity of diffraction peaks. When the NaOH concentration is higher than 0.8 mol/L, the ZSM-5 molecular sieve framework is seriously damaged and presents an amorphous state. Figure 1e shows that the crystal phase structure of the spent catalyst remains unchanged after alkali treatment alone, but the diffraction peak intensity of the sample decreases, indicating that the lattice structure of the ZSM-5 molecular sieve changes after alkali treatment.

2.2. XRF Analysis

According to Tables 1 and 2, the Si/Al ratio of the waste MTP catalyst before acid treatment is only 6.51, and the Si/Al ratios of the samples after acid treatment are significantly increased. At the same concentration, $\text{H}_2\text{C}_2\text{O}_4$ has a better dealuminization effect than HCl and increases the ratio of silicon to aluminum to a greater degree. The reason may be that $\text{H}_2\text{C}_2\text{O}_4$ is a dihydric acid with a complexation effect. In the dealuminization system, $\text{H}_2\text{C}_2\text{O}_4$ has both acidic and complexation effects on the ZSM-5 molecular sieve framework aluminum. With increasing NaOH concentration, the Si/Al ratio decreases, indicating that the alkali treatment significantly removed Si species on the zeolite. Excessive alkali caused

the collapse of the framework structure of ZSM-5 zeolite and caused serious damage to its pore structure.

Table 1. Elemental composition and content of waste catalyst samples after 4 mol/L HCl acid and alkali combined treatment.

Sample	Element Composition (wt%)						SAR
	SiO ₂	Al ₂ O ₃	Fe ₂ O ₃	CaO	SO ₃	TiO ₂	
FMTP-2P	79.02	20.64	0.0291	0.137	0.133	0.047	6.51
FMTP-2 mol/L HCl	85.24	13.9	0.0246	0.324	0.464	0.026	10.41
FMTP-4 mol/L HCl	87.9	11.5	0.019	0.214	0.245	0.034	12.99
FMTP-6 mol/L HCl	88.35	10.8	0.022	0.313	0.479	0.036	13.88
FMTP-4 mol/L HCl + 0.1 mol/L NaOH	87.33	12.2	0.0208	0.16	0.245	0.044	12.17
FMTP-4 mol/L HCl + 0.2 mol/L NaOH	87.85	11.8	0.016	0.15	0.174	0.034	12.66
FMTP-4 mol/L HCl + 0.4 mol/L NaOH	80.87	18.68	0.0277	0.15	0.23	0.051	7.36
FMTP-4 mol/L HCl + 0.8 mol/L NaOH	20.99	78.41	0.085	0.168	0.252	0.102	0.45
FMTP-4 mol/L HCl + 1.2 mol/L NaOH	7.77	91.58	0.0943	0.16	0.275	0.118	0.14

Table 2. Elemental composition and content of samples before and after alkali combined treatment of waste catalyst subjected to 4 mol/L H₂C₂O₄ acid treatment.

Sample	Element Composition (wt%)						SAR
	SiO ₂	Al ₂ O ₃	Fe ₂ O ₃	CaO	SO ₃	TiO ₂	
FMTP-2P	79.02	20.64	0.029	0.137	0.133	0.047	6.51
FMTP-2 mol/L H ₂ C ₂ O ₄	91.08	8.03	0.023	0.332	0.503	0.029	19.25
FMTP-4 mol/L H ₂ C ₂ O ₄	93.71	5.88	0.014	0.157	0.201	0.026	27.09
FMTP-6 mol/L H ₂ C ₂ O ₄	87.66	11.5	0.025	0.329	0.476	0.037	12.94
FMTP-4 mol/L H ₂ C ₂ O ₄ + 0.1 mol/L NaOH	92.41	7.26	0.013	0.129	0.156	0.031	21.64
FMTP-4 mol/L H ₂ C ₂ O ₄ + 0.2 mol/L NaOH	93.85	5.81	0.012	0.139	0.164	0.026	27.46
FMTP-4 mol/L H ₂ C ₂ O ₄ + 0.4 mol/L NaOH	90.36	9.31	0.013	0.127	0.156	0.028	16.50
FMTP-4 mol/L H ₂ C ₂ O ₄ + 0.8 mol/L NaOH	43.73	55.1	0.467	0.181	0.338	0.149	1.35
FMTP-4 mol/L H ₂ C ₂ O ₄ + 1.2 mol/L NaOH	12.7	86.27	0.464	0.16	0.295	0.129	0.25

2.3. Specific Surface Area and Pore Structure Parameters

Table 3 shows that the specific surface area and pore volume of the samples increase after acid treatment, indicating that acid treatment has a great influence on the specific surface area, pore structure, and properties of the spent catalyst. This is mainly because acid treatment removes the surface of the waste catalyst and the amorphous aluminum accumulated in the channels, which exposes a more effective area and creates a smoother surface and channels. The specific surface area of the sample treated with H₂C₂O₄ is larger than that of the sample treated with HCl, which is consistent with the trends in the XRF data. With increasing alkali concentration, the total pore volume, mesoporous specific surface area, and microporous specific surface area of the samples first increase and then decrease. However, when the NaOH concentration is 0.8 mol/L, the total pore volume and mesoporous specific surface area decrease significantly, which may be because the high-intensity desilication process destroyed part of the framework structure of the ZSM-5 molecular sieve.

Table 3. BET-specific surface area and pore structure parameters of samples before and after acid and alkali combined treatment with 4 mol/L HCl and H₂C₂O₄.

Sample	SBET (m ² /g)	Smicro (m ² /g)	Smeso (m ² /g)	Vtotal (cm ³ /g)	Vmicro (cm ³ /g)	Vmeso (cm ³ /g)	Pore Width (nm)
FMTP-2P	303.956	105.549	198.407	0.287	0.051	0.236	3.7714
FMTP-4 mol/L HCl	332.671	103.730	228.940	0.321	0.050	0.271	3.8539
FMTP-4 mol/L HCl + 0.1 mol/L NaOH	411.710	144.580	267.131	0.709	0.063	0.646	6.8857
FMTP-4 mol/L HCl + 0.2 mol/L NaOH	357.638	121.853	235.785	0.436	0.064	0.372	4.8711
FMTP-4 mol/L HCl + 0.4 mol/L NaOH	380.460	97.136	283.325	0.799	0.050	0.749	8.4058
FMTP-4 mol/L HCl + 0.8 mol/L NaOH	174.996	52.078	122.918	0.433	0.025	0.408	9.8956
FMTP-4 mol/L H ₂ C ₂ O ₄	355.558	95.656	259.902	0.327	0.045	0.282	3.6792
FMTP-4 mol/L H ₂ C ₂ O ₄ + 0.1 mol/L NaOH	404.337	143.700	260.636	0.302	0.056	0.246	2.9834
FMTP-4 mol/L H ₂ C ₂ O ₄ + 0.2 mol/L NaOH	426.766	174.458	252.309	0.435	0.071	0.364	4.0732
FMTP-4 mol/L H ₂ C ₂ O ₄ + 0.4 mol/L NaOH	424.101	117.667	306.434	0.938	0.059	0.879	8.8502
FMTP-4 mol/L H ₂ C ₂ O ₄ + 0.8 mol/L NaOH	119.542	32.651	86.891	0.474	0.016	0.458	17.7150

2.4. FT-IR Characterization

As seen from Figure 2a,b, the characteristic diffraction peaks of the ZSM-5 molecular sieve appear at wavenumbers of 449 cm⁻¹, 544 cm⁻¹, 798 cm⁻¹, 1090 cm⁻¹, and 1220 cm⁻¹. Among them, the absorption peak at 449 cm⁻¹ belongs to the bending vibration of X-O bonds in SiO₄ and AlO₄ tetrahedra (X is Si or Al), and the absorption peaks at 544 cm⁻¹ and 1220 cm⁻¹ belong to the vibration of the double five-membered ring in the ZSM-5 molecular sieve structure. The absorption peak at 798 cm⁻¹ is due to the X-O-X symmetric stretching vibration of external connections, and 1090 cm⁻¹ is due to the antisymmetric stretching vibration of X-O-X bonds inside the tetrahedra. With increasing acid concentration, the framework structure of the ZSM-5 molecular sieve essentially does not change [25].

Figure 2c,d shows that the crystallinity of the samples decreases gradually with increasing alkali concentration. When the NaOH concentration reaches 0.8 mol/L, the framework structure collapses, which is consistent with the XRD results in Figure 1. Figure 2e shows that the characteristic diffraction peak intensity of the ZSM-5 molecular sieve framework decreases after alkali treatment alone. From Figure 2f, the pyridine adsorption infrared (Py-IR) spectra indicate that the Brønsted acid (B-acid) and Lewis acid (L-acid) contents of samples treated with HCl and H₂C₂O₄ show a decreasing trend. After acid treatment, part of the nonframework aluminum is removed, resulting in a decrease in the acid content of L-acid centers composed of the nonframework aluminum, and part of the framework aluminum is also removed, resulting in the destruction of the Si-Al-O structure of the ZSM-5 molecular sieve. H₂C₂O₄ treatment not only removes the framework aluminum of ZSM-5 but also removes part of the nonframework aluminum, while HCl mainly removes the framework aluminum of ZSM-5 but has a weak removal effect on the nonframework aluminum.

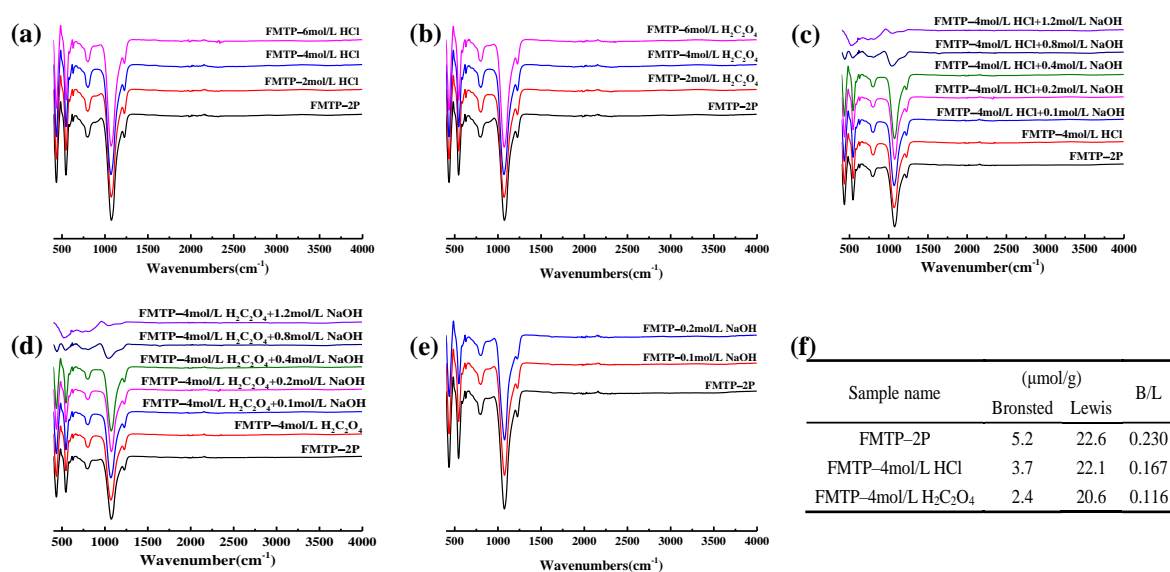


Figure 2. (a) FT-IR diagrams of spent catalyst samples before and after HCl treatment; FT-IR diagrams of spent catalyst samples before and after (b) H₂C₂O₄ treatment; (c) alkali combined treatment of 4 mol/L HCl-treated waste catalyst; (d) alkali combined treatment of 4 mol/L H₂C₂O₄-treated waste catalyst; (e) alkali treatment; (f) Brønsted acid (B-acid) and Lewis acid (L-acid) contents of waste catalysts treated with different acids.

2.5. SEM Characterization

As seen from Figure 3, the samples after acid treatment have an irregular ellipsoidal morphology and uniform grain size, with an average grain size of approximately 1.1 μm, which is similar to the properties of the samples before acid treatment. Alkali treatment destroys the framework structure to a certain extent, and the degree of damage increases with increasing concentration of alkali treatment. When the concentration of NaOH is 0.2 mol/L, a honeycomb structure appears on the surface of the sample, indicating that mesopores are formed by alkali treatment. When the concentration of NaOH is increased further, the mesoporous channels become more obvious. When the concentration of NaOH reaches 0.8 mol/L, the particles are dissolved, and the pore structure collapses, which is consistent with the XRD, XRF, FT-IR, and BET data.

2.6. ²⁷Al MAS-NMR Analysis

Figure 4a,b shows that there are two aluminum species on the waste catalyst before acid treatment. With a general chemical shift, the peak at δ = 50~60 ppm belongs to the signal of the framework aluminum in the ZSM-5 molecular sieve, which has tetrahedral coordination, and the peak at δ = 5.0 ppm belongs to the signal of the hexa-coordinated octahedral nonframework aluminum. There is a shoulder peak at δ = 47.8 ppm, which represents the framework aluminum distributed on the outer surface or large pores of the ZSM-5 molecular sieve. After HCl treatment, the chemical shifts of the two aluminum species in the ²⁷Al NMR spectra do not change, but the peak intensity of the framework aluminum signal decreases at δ = 58.0 ppm, the shoulder at δ = 47.8 ppm disappears, the signal peak intensity of the nonframework aluminum at δ = 5.0 ppm remains unchanged, and the ratio of framework aluminum to the nonframework aluminum decreases, indicating that HCl dealumination mainly removes the framework aluminum from the ZSM-5 molecular sieve. After H₂C₂O₄ treatment, the ²⁷Al NMR spectrum changes significantly. The peak intensity decreases at δ = 5.0 ppm and δ = 58.0 ppm. The shoulder peak at δ = 47.8 ppm is significantly widened, indicating that H₂C₂O₄ not only removes the framework aluminum of the ZSM-5 molecular sieve but also dissolves some of the nonframework aluminum. Therefore, the silicon-to-aluminum ratio after H₂C₂O₄ treatment is greater than that after

HCl treatment, which is consistent with the results of Table 1 and the changes in B-acid and L-acid in Figure 2f.

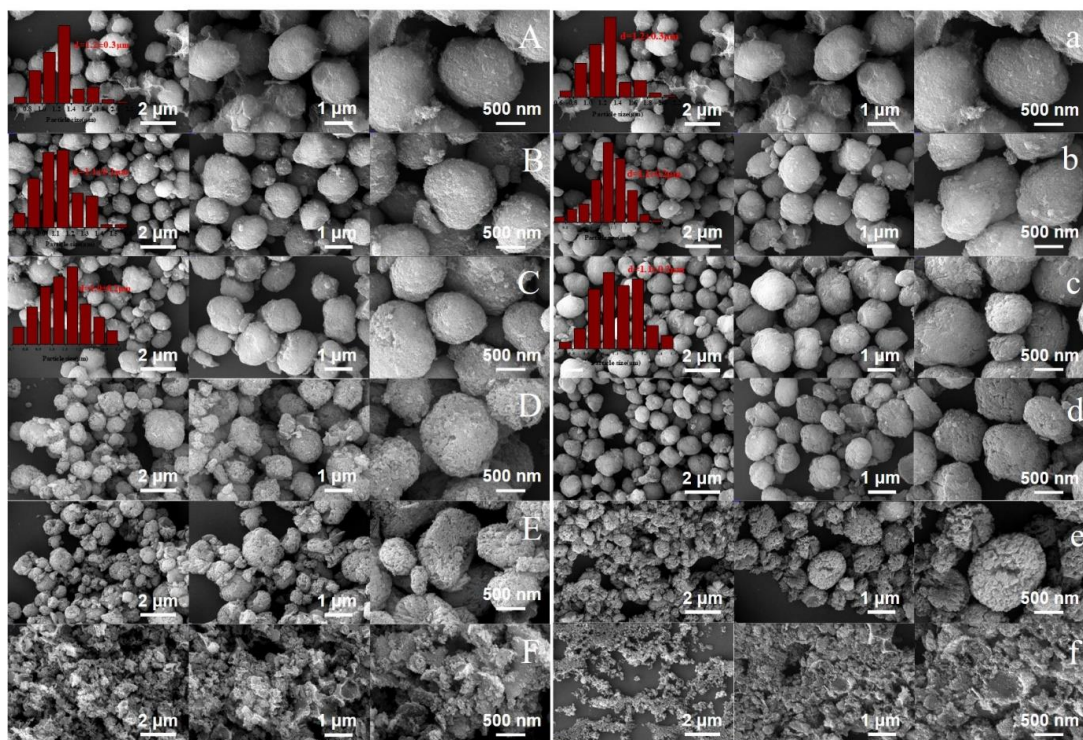


Figure 3. SEM images of (A) FMTP-2P; (B) 4 mol/L HCl; (C) 4 mol/L HCl + 0.1 mol/L NaOH; (D) 4 mol/L HCl + 0.2 mol/L NaOH; (E) 4 mol/L HCl + 0.4 mol/L NaOH; (F) 4 mol/L HCl + 0.8 mol/L NaOH. SEM image of (a) FMTP-2P; (b) 4 mol/L $\text{H}_2\text{C}_2\text{O}_4$; (c) 4 mol/L $\text{H}_2\text{C}_2\text{O}_4$ + 0.1 mol/L NaOH; (d) 4 mol/L $\text{H}_2\text{C}_2\text{O}_4$ + 0.2 mol/L NaOH; (e) 4 mol/L $\text{H}_2\text{C}_2\text{O}_4$ + 0.4 mol/L NaOH; (f) 4 mol/L $\text{H}_2\text{C}_2\text{O}_4$ + 0.8 mol/L NaOH.

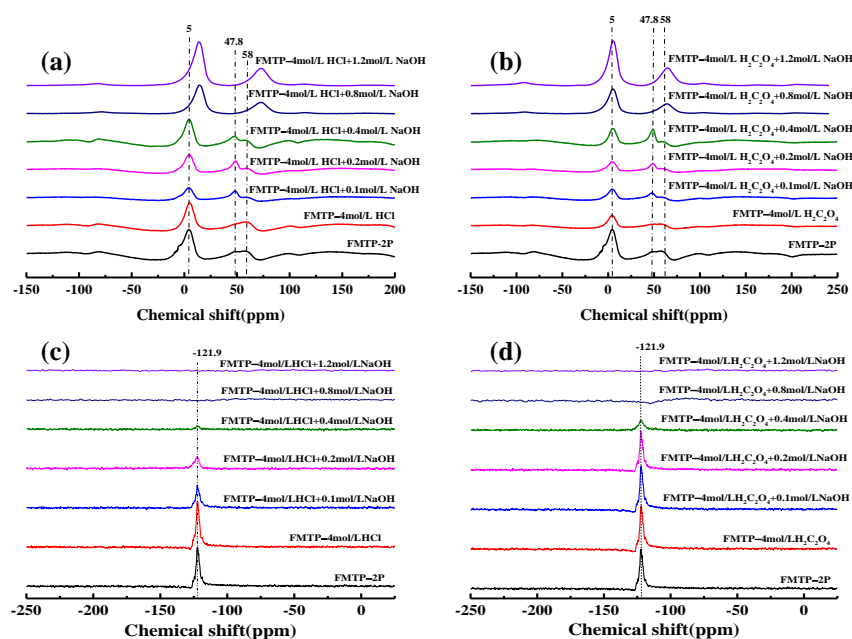


Figure 4. ^{27}Al MAS NMR spectra of waste catalyst samples after (a) 4 mol/L HCl treatment and alkali combined treatment; (b) 4 mol/L $\text{H}_2\text{C}_2\text{O}_4$ treatment and after alkali combined treatment. ^{29}Si MAS-NMR spectra of waste catalyst samples after (c) 4 mol/L HCl and alkali combined treatment; (d) 4 mol/L $\text{H}_2\text{C}_2\text{O}_4$ treatment and alkali combined treatment.

Figure 4c,d shows that after acid treatment, the peak intensity of the silicon signal at $\delta = -121.9$ ppm hardly changes, but the chemical shift moves in the direction of high binding energy, and the shift of the sample treated with $\text{H}_2\text{C}_2\text{O}_4$ is greater than that of the sample treated with HCl. This is because the concentration of aluminum species on the surface of the $\text{H}_2\text{C}_2\text{O}_4$ -treated sample is low, and the electronegativity of aluminum ($\chi = 1.61$) is lower than that of silicon ($\chi = 1.90$). Therefore, the chemical shift is greater. The changes in the spectra of samples treated with different concentrations of alkali are consistent. After treatment with 0.1 mol/L NaOH, the peak intensity of the nonframework aluminum of the ZSM-5 molecular sieve at $\delta = 5.0$ ppm decreases, and the enhanced shoulder signal at $\delta = 47.8$ ppm indicates that alkali treatment further dissolves part of the nonframework aluminum. However, since alkali treatment has the effect of pore expansion, the signal for the framework aluminum in large pores increases. With a further increase in NaOH concentration, the nonframework aluminum signal and shoulder peak aluminum signal gradually increase, the silicon-to-aluminum ratio decreases, the pores collapse, and the aluminum is free in the form of the nonframework aluminum. The peak intensity of the sample after $\text{H}_2\text{C}_2\text{O}_4$ alkali treatment is lower than that of the sample treated with HCl, which is consistent with the XRF data. After acid treatment, the intensity of the silicon peak at $\delta = -121.9$ ppm is almost unchanged. After alkali treatment, the silicon peak decreases, and the chemical shift moves in the direction of high binding energy. When the NaOH concentration reaches 0.8 mol/L, almost no silicon signal can be detected, indicating that the silicon in the sample has been completely dissolved by the high concentration of alkali, and that the framework structure of the ZSM-5 molecular sieve is damaged.

2.7. Adsorption Performance of Waste Catalyst under Acid Treatment

Figures 5 and 6 show that the adsorption capacities of samples treated with HCl and $\text{H}_2\text{C}_2\text{O}_4$ are essentially the same, with values significantly higher than those before treatment. The adsorption capacity increases with increasing acid concentration. When the concentration of acid treatment is 4 mol/L, the adsorption capacity reaches the maximum. When the acid concentration continues to increase to 6 mol/L, the adsorption capacity remains unchanged or even decreases. For a given treatment concentration, the adsorption capacity of samples treated with $\text{H}_2\text{C}_2\text{O}_4$ is greater than that of samples treated with HCl. When $P/P_0 = 0.1$ MPa and the $\text{H}_2\text{C}_2\text{O}_4$ concentration is 4 mol/L, the adsorption capacities of p-xylene and n-hexane reach the maximum, with values of 128.25 mg/g and 103.31 mg/g, respectively, which are 15.4% higher than those of waste catalyst without acid treatment.

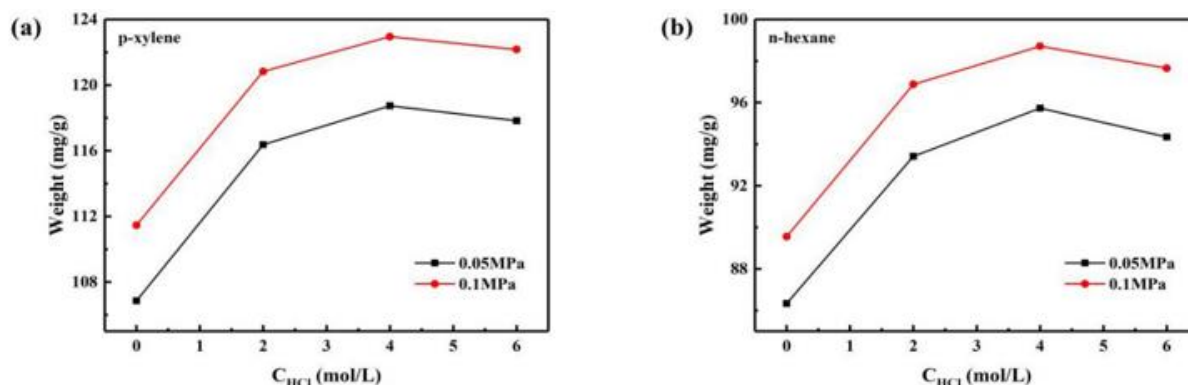


Figure 5. Variation in the adsorption capacities for (a) p-xylene and (b) n-hexane of samples after HCl treatment.

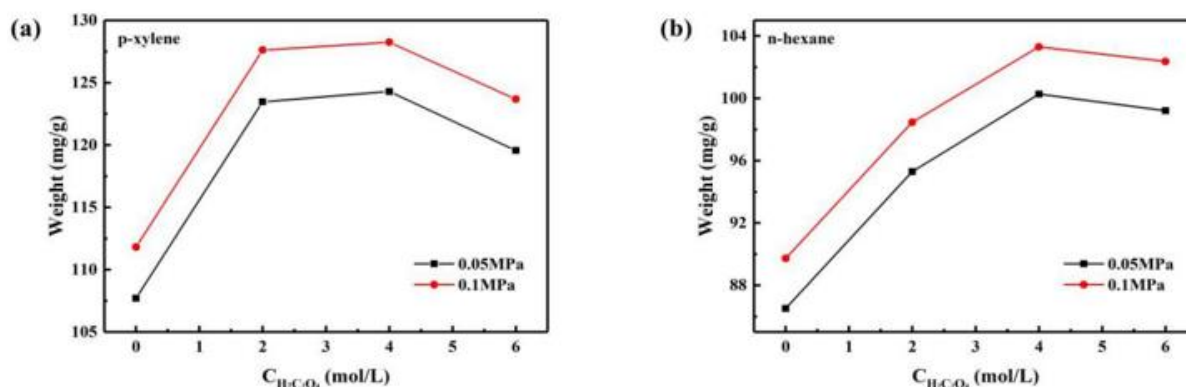


Figure 6. Variation in the adsorption capacities for (a) p-xylene and (b) n-hexane of samples after $\text{H}_2\text{C}_2\text{O}_4$ treatment.

2.8. Change in the Adsorption Rate of Acid-Treated Spent Catalysts under Different Pressures

Figure 7 shows that at the same pressure of 298 K, the amount of p-xylene and n-hexane adsorbed by waste catalyst samples treated with HCl is higher than that of samples treated with $\text{H}_2\text{C}_2\text{O}_4$. The curve of the amount of p-xylene adsorbed over time has the largest slope at $p = 0.5$ KPa, indicating that the sample has the fastest adsorption rate of p-xylene at this pressure. The slope of the corresponding curve for n-hexane is the largest at $p = 13$ KPa, indicating that the adsorption rate for n-hexane is the fastest at this pressure.

2.9. Adsorption Performance of Waste Catalyst Subjected to Acid-Base Combined Treatment

Figures 8 and 9 show that after treatment with 4 mol/L HCl and $\text{H}_2\text{C}_2\text{O}_4$, the amount of p-xylene and n-hexane adsorbed by the waste catalyst after alkali treatment at different concentrations first increases and then decreases. When $P/P_0 = 0.1$ MPa, the $\text{H}_2\text{C}_2\text{O}_4$ concentration is 4 mol/L and the NaOH concentration is 0.1 mol/l, the maximum adsorption capacity of the sample for p-xylene is 141.04 mg/g, and the maximum adsorption capacity for n-hexane is 106.87 mg/g. Compared with the values obtained after acid treatment, the p-xylene and n-hexane adsorption capacities of the samples subjected to combined treatment increase by 5.94% and 6.89% and are 20.7% and 16.2% higher, respectively, than those of waste catalyst without acid and alkali treatment. This shows that after acid-base treatment, the adsorption performance of waste catalysts for VOCs can be further improved.

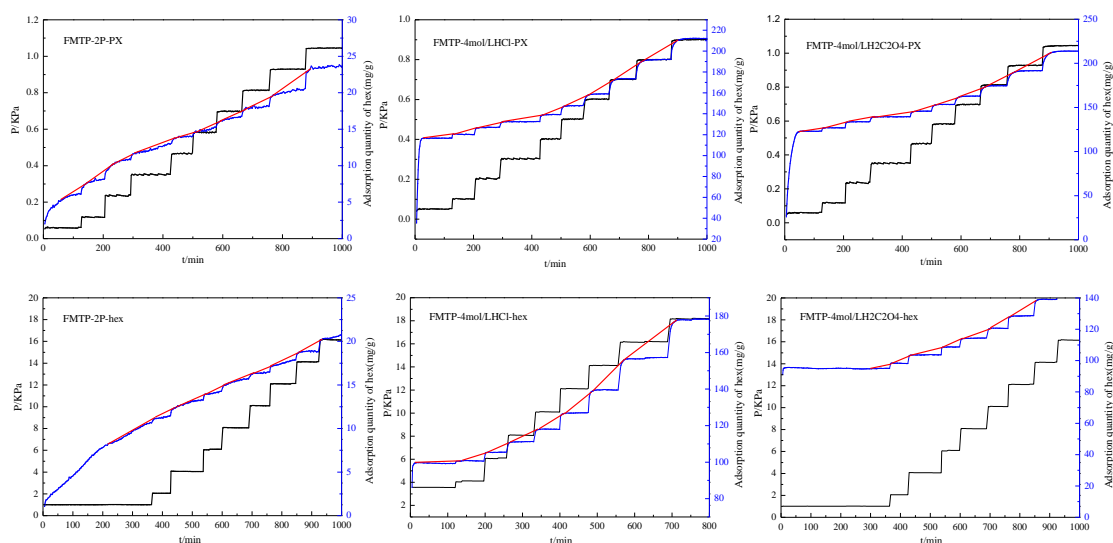


Figure 7. Relationship between sample adsorption capacity and pressure with respect to time before and after HCl and $\text{H}_2\text{C}_2\text{O}_4$ treatment.

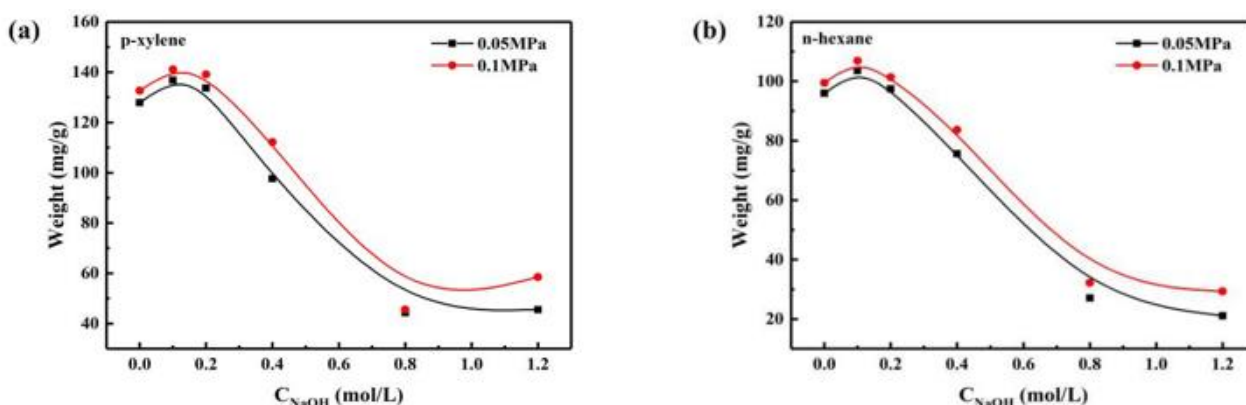


Figure 8. Variation in the adsorption capacities for (a) p-xylene and (b) n-hexane of samples subjected to alkali after $H_2C_2O_4$ treatment.

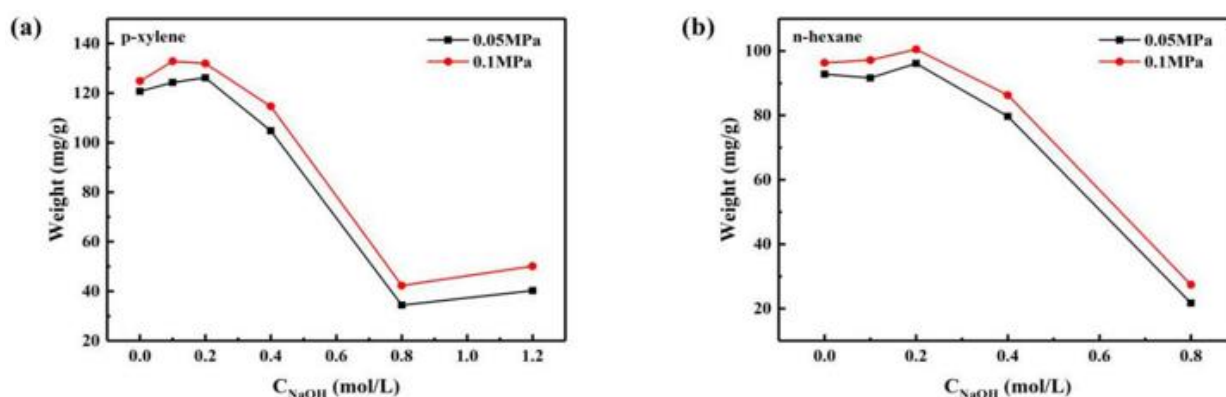


Figure 9. Variation in the adsorption capacities for (a) p-xylene and (b) n-hexane of samples subjected to alkali after HCl treatment.

3. Preparation of a VOC Adsorbent from Waste MTP Catalyst

3.1. Raw Materials

The raw materials were waste fixed-bed MTP (FMTP) catalyst, hydrochloric acid (HCl), oxalic acid ($H_2C_2O_4$), NaOH, HNO_3 solution (68 wt%), deionized water, p-xylene, and n-hexane.

3.2. Preparation of Adsorbent

First, 10 g of spent MTP catalyst powder (below 200 mesh) was added to a water solution of HCl and $H_2C_2O_4$ at concentrations of 2 mol/L, 4 mol/L and 6 mol/L, stirred continuously, and heated at $95\text{ }^\circ\text{C}$ for 4–6 h at constant temperature in a water bath. Next, the solution was centrifuged (8000 r/min, 5 min), washed with deionized water, and dried overnight at $120\text{ }^\circ\text{C}$ in a blower drying box (the corresponding samples are denoted FMTP, FMTP-2 mol/L HCl, FMTP-4 mol/L HCl, FMTP-4 mol/L HCl, FMTP-2 mol/L $H_2C_2O_4$, FMTP-4 mol/L $H_2C_2O_4$, and FMTP-6 mol/L $H_2C_2O_4$). Then, the samples treated with 4 mol/L HCl and $H_2C_2O_4$ were added to 0.1 mol/L NaOH, 0.2 mol/L NaOH, 0.4 mol/L NaOH, 0.8 mol/L NaOH, and 1.2 mol/L NaOH solutions (liquid-to-solid ratio 5:1). Mechanical stirring treatment was conducted in a $95\text{ }^\circ\text{C}$ water bath for 2 h, followed by centrifugation (8000 r/min, 5 min), and the upper waste catalyst mud obtained by centrifugation was then transferred to 250 mL of a 1 mol/L dilute HNO_3 solution under stirring and washing for 30 min to remove the residue after treatment. After washing with deionized water until neutral, the catalyst was put in a blower drying box at $120\text{ }^\circ\text{C}$ overnight to dry and calcined at $600\text{ }^\circ\text{C}$ for 6 h in a muffle furnace. The powder was pressed into pieces and screened to obtain a 14–30 mesh material, and the adsorbent product after acid-base treatment was obtained (the corresponding samples are denoted FMTP-4 mol/L HCl + 0.1 mol/L

NaOH, FMTP-4 mol/L HCl + 0.2 mol/L NaOH, FMTP-4 mol/L HCl + 0.4 mol/L NaOH, FMTP-4 mol/L HCl + 0.8 mol/L NaOH, FMTP-4 mol/L HCl + 1.2 mol/L NaOH, FMTP-4 mol/L H₂C₂O₄ + 0.1 mol/L NaOH, FMTP-4 mol/L H₂C₂O₄ + 0.2 mol/L NaOH, FMTP-4 mol/L H₂C₂O₄ + 0.4 mol/L NaOH, FMTP-4 mol/L H₂C₂O₄ + 0.8 mol/L NaOH, and FMTP-4 mol/L H₂C₂O₄ + 1.2 mol/L NaOH).

3.3. Analysis and Characterization Methods

The crystal structure of the samples was analyzed by X-ray diffraction (XRD, X-pert3 powder diffractometer, Panaco, The Netherlands). The framework structure of the samples was analyzed by Fourier transform infrared spectrometry (FT-IR, Bruker V70, Germany). The Brunauer–Emmet–Teller (BET)-specific surface area and pore properties of the samples were analyzed by a physical adsorption instrument (ASAP2020 surface analyzer, USA). The composition and content of the samples were analyzed via X-ray fluorescence spectroscopy (XRF, Bruker S8 Tiger, Zeiss Merlin, Germany). The micromorphology of the samples was analyzed using a compact scanning electron microscope (SEM, Carl Zeiss, Germany), and the chemical environment of ²⁷Al and ²⁹Si in the samples was determined by nuclear magnetic resonance (NMR, JNM-ECZ600r NMR, Japan). The adsorption properties of the samples for n-hexane, p-xylene, and water were measured with a Beijing Best 3H-2000PW automatic intelligent gravimetric adsorption (IGA) instrument.

4. Conclusions

After acid-base treatment, spent MTP catalyst maintains the crystal structure of the ZSM-5 molecular sieve. With increasing alkali treatment concentration, framework desilication occurs, local structural defect sites are generated in the molecular sieve lattice, and the silicon-to-aluminum ratio of the sample increases; moreover, the dealumination effect of H₂C₂O₄ is better than that of HCl. HCl dealumination mainly removes the framework aluminum of the molecular sieve, while H₂C₂O₄ not only removes the framework aluminum of the molecular sieve, but also dissolves some the nonframework aluminum. The BET-specific surface area and pore diameter of the sample are increased, and the spent catalyst maintains an irregular ellipsoidal shape. After alkali treatment, the surface of the spherical particles becomes rough. With increasing alkali concentration, the damage degree increases. The adsorption of p-xylene and n-hexane by the adsorbent product after acid-base treatment is significantly improved. When P/P₀ = 0.1 MPa, the H₂C₂O₄ concentration is 4 mol/L and the NaOH concentration is 0.1 mol/L, the adsorption capacity of the sample for p-xylene and n-hexane reaches the maximum, with values of 141.04 and 106.87 mg/g, respectively, which are 20.7% and 16.2% higher than those before treatment, showing good adsorption performance.

Author Contributions: X.Y. and Y.M. designed the experiments and wrote the main manuscript text, H.S. analyzed and prepared Figures 1–5, N.Z. analyzed and prepared Figures 6–9. Z.J. and M.Y. revised the manuscript. All authors have read and agreed to the published version of the manuscript.

Funding: This research was financially supported by the State Key Laboratory of High-Efficiency Utilization of Coal and Green Chemical Engineering (2019-KF-08) and the Ningxia Hui Autonomous Region Top Talent Program Funds.

Conflicts of Interest: The authors declare no competing interests.

References

1. Wei, Y.; Parmentier, T.E.; De Jong, K.P.; Zečević, J. Tailoring and visualizing the pore architecture of hierarchical zeolites. *Chem. Soc. Rev.* **2015**, *44*, 7234–7261. [[CrossRef](#)]
2. Betke, U.; Lieb, A. Micro-macroporous composite materials – Preparation techniques and selected applications: A review. *Adv. Eng. Mater.* **2018**, *20*, 1800252. [[CrossRef](#)]
3. Srivastava, R. Synthesis and applications of ordered and disordered mesoporous zeolites: Present and future prospective. *Catal. Today* **2018**, *309*, 172–188. [[CrossRef](#)]

4. Luo, H.; Law, W.W.; Wu, Y.; Zhu, W.; Yang, E.H. Hydrothermal synthesis of needle-like nanocrystalline zeolites from metakaolin and their applications for efficient removal of organic pollutants and heavy metals. *Microporous Mesoporous Mater.* **2018**, *272*, 8–15. [[CrossRef](#)]
5. Cundy, C.S.; Cox, P.A. The hydrothermal synthesis of zeolites: history and development from the earliest days to the present time. *Chem. Rev.* **2003**, *103*, 663–702. [[CrossRef](#)] [[PubMed](#)]
6. Shi, J.; Wang, Y.; Yang, W.; Tang, Y.; Xie, Z. Recent advances of pore system construction in zeolite-catalyzed chemical industry processes. *Chem. Soc. Rev.* **2015**, *44*, 8877–8903. [[CrossRef](#)] [[PubMed](#)]
7. Bayat, M.; Javanbakht, V.; Esmaili, J. Synthesis of zeolite/nickel ferrite/sodium alginate bionanocomposite via a co-precipitation technique for efficient removal of water-soluble methylene blue dye. *Int. J. Biol. Macromol.* **2018**, *116*, 607–619. [[CrossRef](#)]
8. Burakov, A.E.; Galunin, E.V.; Burakova, I.V.; Kucherova, A.E.; Agarwal, S.; Tkachev, A.G.; Gupta, V.K. Adsorption of heavy metals on conventional and nanostructured materials for wastewater treatment purposes: A review. *Ecotoxicol. Environ. Saf.* **2018**, *148*, 702–712. [[CrossRef](#)]
9. Zhang, S.; Gong, Y.; Zhang, L.; Liu, Y.; Dou, T.; Xu, J.; Deng, F. Hydrothermal treatment on ZSM-5 extrudates catalyst for methanol to propylene reaction: Finely tuning the acidic property. *Fuel Process. Technol.* **2015**, *129*, 130–138. [[CrossRef](#)]
10. Chen, X.D.; Li, X.G.; Li, H.; Han, J.J.; Xiao, W.D. Interaction between binder and high silica HZSM-5 zeolite for methanol to olefins reactions. *Chem. Eng. Sci.* **2018**, *192*, 1081–1090. [[CrossRef](#)]
11. Flores, C.; Batalha, N.; Ordonsky, V.V.; Zholobenko, V.L.; Baaziz, W.; Marcilio, N.R.; Khodakov, A.Y. Direct production of iso-paraffins from syngas over hierarchical cobalt-ZSM-5 nanocomposites synthesized by using carbon nanotubes as sacrificial templates. *ChemCatChem* **2018**, *10*, 2291–2299. [[CrossRef](#)]
12. Hu, Z.; Zhang, H.; Wang, L.; Zhang, H.; Zhang, Y.; Xu, H.; Shen, W.; Tang, Y. Highly stable boron-modified hierarchical nanocrystalline ZSM-5 zeolite for the methanol to propylene reaction. *Catal. Sci. Technol.* **2014**, *4*, 2891–2895. [[CrossRef](#)]
13. Yao, L.; Zhou, Y.; Guo, S.; Huangfu, C.; Ma, Y.; Liu, Y.; Yu, Z.; Chen, J.; Jin, K.; Jiang, H.; et al. Comparison of VOCs adsorption performance between Y and ZSM-5 zeolite. *Chin. J. Environ. Eng.* **2022**, *16*, 182–189.
14. Wang, Q.; Yang, Y.; Yu, C.; Huang, H.; Kim, M.; Feng, C.; Zhang, Z. Study on a fixed zeolite bioreactor for anaerobic digestion of ammonium-rich swine wastes. *Bioresour. Technol.* **2011**, *102*, 7064–7068. [[CrossRef](#)]
15. Gruszecka-Kosowska, A.; Baran, P.; Wdowin, M.; Franus, W. Waste dolomite powder as an adsorbent of Cd, Pb(II), and Zn from aqueous solutions. *Environ. Earth Sci.* **2017**, *76*, 521. [[CrossRef](#)]
16. Zhang, Y.; Dong, J.; Guo, F.; Shao, Z.; Wu, J. Zeolite synthesized from coal fly ash produced by a gasification process for Ni²⁺ removal from water. *Minerals* **2018**, *8*, 116. [[CrossRef](#)]
17. Jiménez-Castañeda, M.E.; Medina, D.I. Use of surfactant-modified zeolites and clays for the removal of heavy metals from water. *Water* **2017**, *9*, 235. [[CrossRef](#)]
18. Chen, Y.; Wang, H.; Zhao, W.; Huang, S. Four different kinds of peels as adsorbents for the removal of Cd (II) from aqueous solution: Kinetics, isotherm and mechanism. *J. Taiwan Inst. Chem. Eng.* **2018**, *88*, 146–151. [[CrossRef](#)]
19. Jiang, N.; Shang, R.; Heijman SG, J.; Rietveld, L.C. High-silica zeolites for adsorption of organic micro-pollutants in water treatment: A review. *Water Res.* **2018**, *144*, 145–161. [[CrossRef](#)]
20. Mohamadi, M.; Salimi, F.; Sadeghi, S. Reduction of oil, COD and turbidity of Kermanshah oil refinery effluent using modified nano-zeolite by bismuth and iron. *Desalin. Water Treat.* **2017**, *97*, 151–157. [[CrossRef](#)]
21. Sui, H.; Liu, J.; He, L.; Li, X.; Jani, A. Adsorption and desorption of binary mixture of acetone and ethyl acetate on silica gel. *J. Chem. Eng. Sci.* **2019**, *197*, 185–194. [[CrossRef](#)]
22. Gao, J.; Wang, W.; Zhang, J.; Lei, Z.; Shi, D.; Qu, L. Study on synthesis and adsorption performance of hydrophobic ZSM-5 zeolites for removal of toluene in high-humidity exhaust gas. *CIESC J.* **2020**, *71*, 337–343.
23. Arancibia-Miranda, N.; Baltazar, S.E.; García, A.; Muñoz-Lira, D.; Sepúlveda, P.; Rubio, M.A.; Altbir, D. Nanoscale zero valent supported by zeolite and montmorillonite: Template effect of the removal of lead ion from an aqueous solution. *J. Hazard. Mater.* **2016**, *301*, 371–380. [[CrossRef](#)] [[PubMed](#)]
24. Carrott, M.R.; Russo, P.A.; Carvalhal, C.; Carrott PJ, M.; Marques, J.P.; Lopes, J.M.; Gerner, I.; Guisnet, M.; Ribeiro, F.R. Adsorption of n-pentane and iso-octane for the evaluation of the porosity of dealuminated BEA zeolites. *Microporous Mesoporous Mater.* **2005**, *81*, 259–267. [[CrossRef](#)]
25. Caicedo-Realpe, R.; Pérez-Ramírez, J. Mesoporous ZSM-5 zeolites prepared by a two-step route comprising sodium aluminate and acid treatments. *Microporous Mesoporous Mater.* **2010**, *128*, 91–100. [[CrossRef](#)]
26. Wei, Z.; Xia, T.; Liu, M.; Cao, Q.; Xu, Y.; Zhu, K.; Zhu, X. Alkaline modification of ZSM-5 catalysts for methanol aromatization: The effect of the alkaline concentration. *Front. Chem. Sci. Eng.* **2015**, *9*, 450–460. [[CrossRef](#)]
27. Groen, J.C.; Zhu, W.; Brouwer, S.; Huynink, S.J.; Kapteijn, F.; Moulijn, J.A.; Pérez-Ramírez, J. Direct demonstration of enhanced diffusion in mesoporous ZSM-5 zeolite obtained via controlled desilication. *J. Am. Chem. Soc.* **2007**, *129*, 355–360. [[CrossRef](#)]